Biogeosciences
Discussions

Open Access

Challenges in modelling spatiotemporally varying phytoplankton blooms in the Northwestern Arabian Sea and Gulf of Oman

S. Sedigh Marvasti[1], A. Gnanadesikan[2], A. A. Bidokhti[3], J. P. Dunne[4], and
S. Ghader[3]

[1]Department of Marine Sciences, Science and Research Branch, Islamic Azad University,
Tehran, Iran
[2]Department of Earth and Planetary Sciences, John Hopkins University, Olin Hall, 3400 N.
Charles St., Baltimore, MD 21218, USA
[3]Institute of Geophysics, University of Tehran, Tehran, P. O. Box 14155-6466, Iran
[4]National Oceanic and Atmospheric Administration/Geophysical Fluid Dynamics Laboratory,
201 Forrestal Rd., Princeton, NJ 08540-6649, USA

Correspondence to: S. Sedigh Marvasti (safoora.seddigh@gmail.com)

Discussion Paper | Discussion Paper | Discussion Paper | Discussion Paper |

BGD

12, 9651–9693, 2015

Blooms in the
Northwestern
Arabian Sea and Gulf
of Oman

S. Sedigh Marvasti et al.

Title Page

Abstract   Introduction

Conclusions   References

Tables   Figures

◀◀   ▶▶

◀   ▶

Back   Close

Full Screen / Esc

Printer-friendly Version

Interactive Discussion

Abstract

We examine interannual variability of phytoplankton blooms in northwestern Arabian Sea and Gulf of Oman. Satellite data (SeaWIFS ocean color) shows two climatological blooms in this region, a wintertime bloom peaking in February and a summertime
5 bloom peaking in September. A pronounced anti-correlation between the AVISO sea surface height anomaly (SSHA) and chlorophyll is found during the wintertime bloom. On a regional scale, interannual variability of the wintertime bloom is thus dominated by cyclonic eddies which vary in location from one year to another. These results were compared against the outputs from three different 3-D Earth System models.
10 We show that two coarse (1°) models with the relatively complex biogeochemistry (TOPAZ) capture the annual cycle but neither eddies nor the interannual variability. An eddy-resolving model (GFDL CM2.6) with a simpler biogeochemistry (miniBLING) displays larger interannual variability, but overestimates the wintertime bloom and captures eddy-bloom coupling in the south but not in the north. The southern part of the
15 domain is a region with a much sharper thermocline and nutricline relatively close to the surface, in which eddies modulate diffusive nutrient supply to the surface (a mechanism not previously emphasized in the literature). We suggest that for the model to simulate the observed wintertime blooms within cyclones, it will be necessary to represent this relatively unusual nutrient structure as well as the cyclonic eddies. This is a
20 challenge in the Northern Arabian Sea as it requires capturing the details of the outflow from the Persian Gulf.

1 Introduction

The region of northwestern Arabian Sea and the Gulf of Oman (15–26° N, 56–66° E) is a highly productive region (Madhupratap et al., 1996; Tang et al., 2002), with satellite
25 estimates of carbon export of $137\,\mathrm{g\,C\,m^{-2}\,yr^{-1}}$, much higher than the $\sim 80\,\mathrm{g\,C\,m^{-2}\,yr^{-1}}$ found in the Subpolar North Atlantic and Pacific (Dunne et al., 2007). Peak chloro-

phyll *a* concentrations exceed 0.7 mg m^{-3} in this region (Fig. 1a). The Arabian Sea is influenced by a reversing monsoonal cycle (Wang and Zhao, 2008), an evaporative fresh-water flux over most of the basin, and an annual mean heat gain (Banse and McClain, 1986; Fischer et al., 2002). In summer (June–September), the southwest Monsoon (SWM) blows strongly across the northwestern Arabian Sea (Al-Azri et al., 2010). Driven by a land–sea pressure gradient, the SWM is a large-scale feature of the atmospheric circulation of the tropics, extending from a surface pressure high near 30° S in the Southern Hemisphere northward to the surface low over Asia (Anderson and Prell, 1993). During the SWM, winds are steered by the East African highlands to form a strong low level atmospheric jet, referred to as the Findlater Jet (Bartolacci and Luther, 1999; Honjo et al., 2000), which crosses the Equator over the Indian Ocean and blows over the Arabian Sea parallel to the Omani coastline in a northeast direction (Honjo et al., 2000). The orientation of the Findlater Jet parallel to Omani coast leads to coastal upwelling along the coast and downwelling on the eastern side of the Jet in the middle of Arabian Sea. This upwelling provides nutrients to the surface layer (Fig. 1b) (Al-Azri et al., 2013; Kawamiya and Oschlies, 2003; Madhupratap et al., 1996; Murtugudde et al., 2007; Veldhuis et al., 1997; Wang and Zhao, 2008). The SWM does not destabilize the surface layers, which are fairly stable in northern summer (Fig. 1c).

The Northeast Monsoon (NEM), which happens from December through February, is not as strong as the SWM (Dickey et al., 1998; Shalapyonok et al., 2001; Veldhuis et al., 1997). Ocean surface wind stress is lower (0.032 N m^{-2} in NEM compared to 0.127 N m^{-2} in SWM), and does not lead to upwelling like the SWM along the Omani coast. However, negative heat flux results in a destabilizing buoyancy flux, subsequent convective overturning (Barimalala et al., 2013; Kawamiya and Oschlies, 2003), and deepening and cooling of the mixed layer to a depth of $\sim$ 80 m (Fig. 1c). This brings up nutrients and fuels a wintertime bloom.

Harmful algae blooms (HABs) and so-called Red Tides have recently affected the coastal regions, aquatic life, water resources, tourism, and fisheries industries of the countries around the region, particularly Iran and Oman. During and following the

Blooms in the Northwestern Arabian Sea and Gulf of Oman

S. Sedigh Marvasti et al.

Back   Close

Full Screen / Esc

Printer-friendly Version

Interactive Discussion

2008–2009 long-lasting red tide in the Persian Gulf and the Gulf of Oman, several site specific studies were done mostly by the researchers in the nearby countries. These included both field studies and remote sensing measurements. The red tide lasting nearly 8 months starting in September 2008 was the first harmful algal bloom of *Cochlodinium polykrikoides* (an American/Malaysian ribo-type distributed worldwide). This bloom began in the Strait of Hormuz and the Gulf of Oman and was then advected to the inner Persian Gulf (Fatemi et al., 2012; Hamzehei et al., 2012; Richlen et al., 2010). HAB occurrences have been more frequently reported in the Gulf of Oman rather than Persian Gulf. A total of 66 red tide events (mostly dominated by *Noctiluca scintillans*) have been recorded between 1976 and 2004 including 25 blooms resulting in mass mortality of fish and marine organisms. In both the Persian Gulf and the Gulf of Oman, there is evidence that HABs and their impacts are increasing (Richlen et al., 2010) due to aquaculture activities and industrial and sewage inputs, natural dispersal and human-aided transport, long-term increases in nutrient loading and global expansion of species (Richlen et al., 2010).

The blooms highlighted in Fig. 1 are mostly nutrient driven with bloom months correlated with higher nitrate (Fatemi et al., 2012). The unusual occurrence of *C. polykrikoides* in the Persian Gulf superseded the more frequently occurring bloom species, *Noctiluca scintillans*, in 2008–2009. Al-Azri et al. (2013) proposed several reasons for this bloom including: stronger upwelling along the Iranian and northern Omani coasts during the southwest monsoon, discharge of unusually warm coastal plume water along the coast of Oman with the reversal of monsoonal winds, and elevated nutrient load higher than that observed in the previous year.

One factor that affects the distribution of plankton blooms in the Northwest Arabian Sea is mesoscale eddy activity (Al-Azri et al., 2013; Dickey et al., 1998; Hamzehei and Bidokhti, 2013; Shalapyonok et al., 2001). The confluence of the Persian Gulf outflow current and the East Arabian Sea Current parallel to Omani and Yemeni coastlines in Arabian Sea leads to formation of a frontal zone and formation of persistent eddies in the region. Because the size of eddies is comparable to the width of the Gulf of

Blooms in the Northwestern Arabian Sea and Gulf of Oman

S. Sedigh Marvasti et al.

Oman, they can affect mixing and transport of biota on a basin scale (Fischer et al., 2002; Piontkovski et al., 2012). Piontkovski et al. (2012) suggested that the increased amplitude of the seasonal cycle of chlorophyll *a* might be associated with the increased variability of mesoscale eddy kinetic energy (EKE) per unit mass in the Gulf of Oman
5 or in the western Arabian Sea.

The potential for eddies to have a significant impact on the ecological, biological and chemical cycles of the upper ocean has been much studied in recent years (Dickey et al., 1998; Eden et al., 2009; McGillicuddy et al., 2001). Eddies can lift nutrient-rich water from the lower layers to the upper-ocean level within the euphotic zone
10 (McGillicuddy et al., 1998). Eddy pumping can also provide the nutrient supply required for bloom formation.

Three different eddy structures have been identified, namely: (1) cyclones, (2) anticyclones, and (3) mode-water eddies, based on the different characteristic vertical structure of the subsurface layers. In a cyclonic eddy, both the seasonal and perma-
15 nent thermocline are lifted up (Kumar et al., 2001), producing a cold SST anomaly (Al-Azri et al., 2010; Banse and English, 1993; Banse and McClain, 1986; Tang et al., 2002; Wiggert et al., 2002). Local increase of the water density also causes a negative sea-level anomaly (SLA) (McGillicuddy et al., 1998). Anticyclones are associated with clockwise rotation in the Northern Hemisphere, warm temperature anomalies, high
20 sea surface anomalies, deepening of both the seasonal and permanent thermocline, and downwelling of isopycnals that pushes low-nutrient water through the base of the euphotic zone (Ewart et al., 2008; Piontkovski et al., 2012). Cyclonic eddies are associated with the opposite characteristics and notably strong nutrient supply into the euphotic zone. All the above characteristics of the cyclonic and anticyclonic eddies
25 are intensified by the interaction of two adjacent eddies of opposite sign (McGillicuddy et al., 2007). A mode-water eddy can be identified by upward displacement of the seasonal thermocline and downward displacement of the main thermocline. As the main thermocline perturbation dominates the geostrophic flow, these eddies are marked by CW rotation with elevated sea surface anomalies like anticyclones but, in contrast to

the anticyclones, they are associated with a shoaling the isopycnal (upwelling) and a cold-water anomaly near the surface (Sweeney et al., 2003).

There are two distinct ways by which eddies have been argued to provide a systematic transfer of tracer and nutrients on isopycnals: advective transfer (slumping isopycnals) and diffusive transfer (down-gradient diffusion). It has been argued that advection rather than diffusion is the dominant process (Banse and McClain, 1986; Lee and Williams, 2000; Lee et al., 2007). In addition, the eddy transfer of heat may lead to mixed layer shallowing, which in turn can lead to an earlier onset of the spring bloom due to more light (Lee and Williams, 2000; Levy et al., 1998). Eddy/wind interactions amplify the eddy-induced upwelling in mode-water eddies, but dampen eddy-induced upwelling in cyclones (McGillicuddy et al., 2007).

It has been argued that mesoscale eddy activity is the dominant mode of nutrient transport in interior of subtropical gyres (Eden et al., 2009; Ewart et al., 2008; McGillicuddy et al., 2001, 1998, 1999, 2007; Sweeney et al., 2003). At the Bermuda Atlantic Time-series Study (BATS) site both cyclonic and mode-water eddies have been associated with an accumulation of phytoplankton biomass and organic matter (Ewart et al., 2008). As observed in the lee of Hawaii during field experiments in 2005, blooms characterized by high chlorophyll *a* concentration can happen within the "senescent" diatoms and Deep chlorophyll *a* Maximum Layer (DCML) which are between the surface mixed layer dominated by small phytoplankton and the deep layer characterized by decreasing phytoplankton activity (Nencioli et al., 2010).

The purpose of this paper is to examine interannual variability of phytoplankton blooms in northwestern Arabian Sea and to determine whether the latest generation of Earth System Models is capable of simulating both the blooms and their variability (allowing for bloom frequency to be projected into the future). We begin by examining blooms in the northwestern Arabian Sea and the Gulf of Oman as seen in ocean color estimated from satellite and relating this to the eddy field as seen in the sea surface height. We find a seasonal relationship between eddies and chlorophyll such that cyclonic eddies are associated with blooms, but only during the winter. This means that

Full Screen / Esc

Printer-friendly Version

Interactive Discussion

interannual variability in blooms will be shaped by mesoscale eddy activity and may not be predictable. We then examine the challenges faced by global Earth System Models (ESMs) in simulating these blooms by comparing the data with output from different ESMs. Two coarse-resolution models with a relatively complex biogeochemistry (TOPAZ) capture the annual cycle but neither eddies nor the small-scale interannual variability. The GFDL CM2.6 eddy-resolving model with a simplified biogeochemistry (miniBLING) produces more interannual variability, but overestimates the wintertime bloom and captures eddy-bloom coupling in the south but in the north. Accordingly, the models do not simulate this relationship except in a few special cases. We argue that in the real world eddies act to modulate turbulent mixing of nutrients to the surface during the NEM. However, this mechanism can only act if there is a strong and relatively shallow nutricline. Since the high resolution model simulates a warm water input from the Persian Gulf that is too close to the surface, it does not capture the observed relationship between SSH and biology in the Northern Arabian Sea.

2 Description of data and models

2.1 Satellite products

We examine the relationship of blooms and eddies using the GSM5 Maritorena et al. (2002) product based on the SeaWIFS (Sea-viewing Wide Field-of-view Sensor) ocean color data and Sea Surface Height Anomaly (SSHA), based on altimeter data acquired from the Archiving, Validation and Interpretation of Satellite Oceanographic (AVISO) Data Center (http://www.aviso.oceanobs.com). The SSH anomaly is calculated relative to the annual cycle.

The GSM algorithm represents the normalized water leaving radiance $L_{wN}(\lambda)$ at multiple wavelengths as a nonlinear function, as following (Maritorena et al., 2002),

$$\hat{L}_{wN}(\lambda) = \frac{tF_0(\lambda)}{n_w^2} \times$$

$$\sum_{i=1}^{2} g_i \left\{ \frac{b_{bw}(\lambda) + b_{bp}(\lambda_0)(\lambda/\lambda_0)^{-\eta}}{b_{bw}(\lambda) + b_{bp}(\lambda_0)(\lambda/\lambda_0)^{-\eta} + a_w(\lambda) + \mathrm{Chl}\, a_{Ph}^*(\lambda) + a_{cdm}(\lambda_0)\exp[-S(\lambda - \lambda_0)]} \right\}^{i} \quad (1)$$

where t is the sea–air transmission factor, $F_0(\lambda)$ is the extraterrestrial solar irradiance, n_w is the index of refraction of the water, seawater backscatter $b_{bw}(\lambda)$, absorption $a_w(\lambda)$, a_{ph}^* is the chlorophyll a (chl) specific absorption coefficient, S is the spectral decay constant for absorption by chromophoric dissolved organic materials (CDOM), η is the power-law exponent for the particulate backscattering coefficient, and λ_0 is a scaling wavelength (443 nm). The cdm absorption coefficient $[a_{cdm}(\lambda_0)]$, and slope factor S then determine the absorption across a range of wavelengths while the particulate backscatter coefficient $[b_{bp}(\lambda_0)]$ and coefficient η constrain the scattering. Letting λ_0 be 443 nm assuming that all terms other than chl, $[a_{cdm}(\lambda_0)]$ and b_{bp} (443 nm) are constant, one can then use the water leaving radiance to invert for chl, a_{cdm}, and backscatter. One limitation of this approach is that if the inherent optical properties vary with time, this variation will introduce errors into the estimate. Following Behrenfeld et al. (2005), we convert the backscatter coefficient into units of particulate carbon biomass using the relationship $p_{carb} = 13\,000(b_{bp} - 0.00035)$.

Satellite-based remote sensing is the only observational method suitable for measuring physical and biological properties over large regions of the ocean. However, satellite ocean color and SST are limited to surface distributions and provide no information about the vertical structure within the ocean (McGillicuddy et al., 2001). Additionally acquiring data requires cloud-free viewing of the ocean surface, which as we will see is a problem in this region at certain times of the year. This lack of information motivates our examination of numerical models, which ideally could be used to provide

estimates of the ocean state when observations are sparse as well as to extrapolate both vertically and into the future.

2.2 Numerical models

Numerical results are presented in this paper based on the output of three different 3-D global Earth system models, which we denote CORE-TOPAZ, Coupled-TOPAZ and GFDL CM2.6 (miniBLING). The first two of these models use the relatively complex TOPAZ biogeochemistry, but have low resolution and do not resolve eddies, while the last model has very high resolution, but a much simpler biogeochemistry.

The TOPAZ code (Tracers of Ocean Productivity with Allometric Zooplankton code of Dunne et al., 2010), keeps track of five inorganic nutrients used by phytoplankton: nitrate and ammonia, inorganic phosphate, silicate, and dissolved iron. Additionally, the model carries three other dissolved inorganic tracers: dissolved inorganic carbon, alkalinity and dissolved oxygen. Based on the work of Dunne et al. (2007), the model also keeps track of fine lithogenic material, which plays a role in ballasting organic material and delivering it to the sediment (Armstrong et al., 2002; Klaas and Archer, 2002). The five inorganic nutrients are taken up in different ways by three classes of phytoplankton: small, large and diazotrophic. A comprehensive description of TOPAZ v2 can be found in the supplemental material of Dunne et al. (2013).

The ocean-ice model used in the CORE-TOPAZ model follows the corresponding components of the GFDL CM2.1 global coupled climate model (Delworth et al., 2006). The vertical resolution ranges from 10 m over the top 200 m to a maximum thickness of 250 m at 5500 m depth with 50 layers in all. The meridional resolution is 1°, whereas the zonal resolution varies between 1° in mid-latitudes and 1/3° at the equator. North of 65°, a tripolar grid is employed to avoid singularity arising from convergence of meridians at the North Pole. Up-to-date parameterizations of mixed-layer dynamics, isopycnal mixing, advection by subgridscale eddies, bottom topography, bottom flows, and lateral viscosity are included- for more detail see Griffies et al. (2005) and Gnanadesikan

Title Page

Abstract · Introduction

Conclusions · References

Tables · Figures

|◄ · ►|

◄ · ►

Back · Close

Full Screen / Esc

Printer-friendly Version

Interactive Discussion

et al. (2006). Both the dynamics and thermodynamics sea ice are simulated with of five thickness classes of sea ice being resolved.

In the CORE-TOPAZ model, surface forcing is set using the Coordinated Ocean-ice Reference Experiment (CORE) protocol (Griffies et al., 2009), where the inputs for calculating surface fluxes are taken from an atmospheric analysis dataset adjusted to agree better with in situ measurements. Sensible and latent heat fluxes are then calculated using bulk formulae. Freshwater forcing is given by a combination of applied precipitation, evaporation computed using bulk fluxes, and a correction diagnosed to restore surface salinities in the top 10 m to climatological monthly values over 60 d. Hence, the fluxes forcing the CORE runs could be thought of as "best guess" observationally based estimates. Such a prescription omits important feedbacks whereby the atmosphere ensures that rainfall and evaporation are consistent with each other, although the restoring correction is a crude representation of these feedbacks. We use the version of the model described in Gnanadesikan et al. (2011), which analyzed different modes of interannual variability in biological cycling across the Pacific Ocean.

The Coupled-TOPAZ model corresponds to the control simulation of the GFDL ESM2M submitted as part of the IPCC AR5 process (Dunne et al., 2012). In this model the ocean is coupled to the atmosphere, land, and sea ice components. Gnanadesikan et al. (2014) discuss the behavior of this model in the North Atlantic, but its behavior in the Arabian Sea has not been previously analyzed.

The ocean component of ESM2M employs the MOM4p1 code of Griffies et al. (2009) which largely mimics the CM2.1 ocean (identical horizontal and vertical resolution and parameterization of mixing). However, ESM2M ocean uses a rescaled geopotential vertical coordinate (z^*; Adcroft et al., 2004; Stacey et al., 1995) for a more robust treatment of free surface undulations.

The ESM2M implementation includes updates to the K-profile parameterization (Large et al., 1994) based on Danabasoglu et al. (2006), as well as model-predicted chlorophyll modulation of short-wave radiation penetration through the water column. ESM2M also includes completely novel parameterizations relative to CM2.1, such

Blooms in the Northwestern Arabian Sea and Gulf of Oman

S. Sedigh Marvasti et al.

Full Screen / Esc

Printer-friendly Version

Interactive Discussion

Discussion Paper | Discussion Paper | Discussion Paper | Discussion Paper

as parameterization of submesoscale eddy-induced mixed layer restratification (Fox-Kemper et al., 2008). Instead of prescribed vertical diffusivity for interior mixing (Bryan and Lewis, 1979), ESM2M employs the Simmons et al. (2004) scheme along with a background diffusivity of $1.0 \times 10^{-5}\,\mathrm{m^2\,s^{-1}}$ in the tropics and $1.5 \times 10^{-5}\,\mathrm{m^2\,s^{-1}}$ pole-ward of 30° latitude following a tanh curve.

The Geophysical Fluid Dynamics Laboratory Climate Model version 2.6 (CM2.6) is a high-resolution eddy-resolving model. This model has the same atmosphere model and ocean Physics as CM2.5 (Delworth et al., 2012). CM2.6's ocean component has higher horizontal resolution than CM2.5, with grid spacing, which is changeable from 11 km at the equator to less than 4 km at very high latitudes. This means that the model is capable of resolving eddy features in the tropics, as we will see below.

Biological cycling in CM2.6 is simulated using a modified version of the Biogeochemistry with Light Iron Nutrients and Gasses (BLING) model (Galbraith et al., 2010) called mini-BLING (Galbraith et al., 2015). The original version of BLING has only five explicit tracers: dissolved inorganic phosphorus (PO_4), dissolved organic phosphorus (DOP), dissolved Iron (Fe), DIC (dissolved inorganic carbon), and oxygen (O_2). It includes the impacts of macronutrient and micronutrient limitation and light limitation on phytoplankton by using these to calculate a growth rate. It then uses this growth rate and implicit treatment of community structure to estimate phytoplankton biomass, and uses this biomass to calculate the rate at which nutrient is taken up by plankton and cycled through the ecosystem. In miniBLING, the iron field is taken from a lower-resolution version of the model (an approximation which has limited impact in the Arabian Sea, where phytoplankton are generally not iron-limited) and so Fe is not treated prognostically. Simulations using the ESM2M physical model show that control simulations of oxygen and surface nutrients produced by miniBLING and BLING models are very similar to those produced in the same model with TOPAZ (Galbraith et al., 2015). This manuscript also shows that BLING and miniBLING simulate very similar patterns of oxygen change and anthropogenic uptake in a simulation where CO_2 is increased by 1 % year^{-1} until it doubles.

Full Screen / Esc

Printer-friendly Version

Interactive Discussion

It should be noted that BLING neglects some processes that may be important. Only nonliving components are advected and mixed by the ocean circulation, which could result in inaccurate distribution of biology in frontal regions at high resolution. Also, the rich behavior of the nitrogen cycle with its interaction with iron, phosphorus and oxygen
5 cannot be simulated with one macronutrient tracer. Specifying iron limitation, as done in miniBLING, may also have some impacts in our region. As extensively discussed by (Naqvi et al., 2010) there is a possibility of iron limitation over the southern parts of the Omani shelf and in the offshore region during the latter part of the Southwest Man-soon, which can result in high nitrate-low chlorophyll conditions. The western equatorial
10 and southern tropical region of the Indian Ocean are iron-limited and the Arabian Sea (southern parts) may become iron-limited under strong upwelling conditions (Wiggert et al., 2006).

3 Remote sensing results

3.1 Interannual variability

15 Using the GSM5 satellite data, the temporal variation of variability of chlorophyll *a* in mesoscale structures in two different regions, including whole region (56–66° E, 15–26° N) and a smaller region, particularly Oman Sea, (60–62° E, 22–26° N) are consid-ered to study the annual cycles. As shown in Fig. 2a–c for whole region, clear annual cycles of chlorophyll *a*, backscattering and CDOM are observed. Even clearer annual
20 cycles of variation of chlorophyll *a*, backscattering and CDOM results are seen in the smaller region, as shown in Fig. 2d–f. More pronounced interannual variability is ob-served in the smaller region as opposed to the larger region.

The annual variations of all parameters are systematically consistent with each other. The maximum values that can be considered as a summer bloom mostly happen in
25 September, with values of $1.0\,\mathrm{mg\,m^{-3}}$, $50\,\mathrm{mg\,C\,m^{-3}}$, and $0.1\,\mathrm{m^{-1}}$ for chlorophyll, par-ticulate carbon and CDOM, respectively, within the whole region and $1.25\,\mathrm{mg\,m^{-3}}$,

65 mg C m^{-3}, and 0.125 m^{-1} for chlorophyll, particulate carbon, and CDOM, respectively, within the smaller region. For two years of 2001 and 2002, the particulate carbon values ($\sim$ 90 mg C m^{-3}) are much higher that the average of the other months over both regions, but the chlorophyll does not show pronounced peaks. A winter bloom is also pronounced in February as a second maximum in a yearly cycle, where the magnitudes are about 0.07 mg m^{-3}, 40 mg C m^{-3}, and 0.07 mg C m^{-3} for chlorophyll, particulate carbon and CDOM, respectively, within the whole region, and about 0.09 $\sim$ 1.5 mg m^{-3}, 55 $\sim$ 80 mg C m^{-3}, and 0.11 $\sim$ 0.14 mg C m^{-3} for chlorophyll, particulate carbon and CDOM, respectively, within the smaller region. Accordingly, the summer bloom in the both regions is stronger than the winter bloom as also discussed by Al-Azri et al. (2010) and Levy et al. (2007).

3.2 Variability of chlorophyll *a* in mesoscale structures

Mesoscale structures can be seen in the Northwest Arabian Sea in both the SeaWiFS chlorophyll *a* distribution and AVISO sea surface height anomaly. During the particular year of 2001 (Fig. 3), both a summer bloom (which most likely starts in August and ends in $\sim$ October) and a winter bloom (which starts in January and goes away in April) can be seen in chlorophyll *a*. In March, the last month of the winter bloom, chlorophyll *a* concentrations are high over the entire region in both the anticyclones (warm eddies with positive SSHA) and the cyclones (cold eddies with negative SSHA). The observed bloom in March terminates abruptly in April, although the observations show that eddies are still active in the region. In June, July and August, the satellite ocean color data is not available due to excessive cloudiness. In September, the last month of the summer bloom, most of the region including cyclones and anticyclones and coastal regions had high chlorophyll *a* concentration. However in the following months the bloom persists only within the cold eddies and disappears over the warm eddies (a phenomenon also seen in Sargasso Sea by McGillicuddy et al., 2001).

The relationship between high chlorophyll *a* and eddies for the other years between 1998 and 2005, is examined qualitatively in Fig. 4. The months with blooms (defined as having local concentrations of chlorophyll $> 1\,\mathrm{mg\,m^{-3}}$) have been shown with different colors, showing whether blooms are found within the cyclones (blue), anticyclones (red) or even both (both blue and red). Months with no data are shown with grey colors and the months with no observed blooms are just kept white. Blooms are observed throughout northern fall and winter similar to the previous findings (Kawamiya and Oschlies, 2003; Levy et al., 2007). Blooms are found both cyclones and anticyclones in several months (every March and September for which we have data, most Februaries) suggesting that the nutrient supply is not modulated by eddies during these months. In April high chlorophyll is not found anywhere within the basin. Blooms are primarily found within cyclonic eddies during the months of November and December, with some association in October and January.

The eddy-chlorophyll relationship clearly changes over the course of the year. During the late wintertime (February to March) the connection between the regional eddies and the chlorophyll concentration is not clear and it seems that the bloom goes away in April over the entire region. The bloom collapse in April could be caused by the shut-off of the relatively weak northeast Monsoon, which results in stopping the vertical mixing and convective overturning. Insofar as the blooms are more driven by the nutrients, the resulting nutrient deficit in euphotic zone would be expected to cause a collapse in production in the Northwest Arabian Sea. In September, which is the last month of the summer bloom, high chlorophyll concentrations are seen in both cyclonic and anticyclonic eddies but in the following months blooms are found only within cyclonic eddies during the months of November and December, with some association in October and January.

3.3 Chlorophyll–Sea Surface Height Anomaly (SSHA) cross-correlation

The seasonal relationship between chlorophyll and SSHA can be seen in monthly variation of the spatial cross-correlation between the two variables over the entire north-

west Arabian Sea. Chlorophyll–SSHA cross-correlations between 1998 and 2005 in the satellite data are shown in Fig. 5a. To check that the chlorophyll results are not an artifact of the remote sensing inversion, two other related parameters, the backscattering coefficient (BBP) and chromophoric dissolved organic matter (CDOM) are also cross-correlated with SSHA, as depicted in Fig. 5b and c. The results show consistent annual cycles of variation in the cross-correlation of all three variables. This suggests a repeatable yearly phenomenon in the region as discussed in the previous sections. The cross-correlation results over 8 years of study shows that there are several months (i.e. November–December) with relatively high anti-correlation for most of the years and also several other months (i.e. April–May) with no or even low positive correlation.

The averaged climatological monthly cross-correlation with SSHA and climatological monthly values between 1998 and 2005 are shown in Fig. 6 for all parameters. Comparing the average values of chlorophyll a over the region and the corresponding cross-correlation with SSHA reveals consistent results with the qualitative approach discussed in the previous section. Two blooms ending in March (winter) and September (summer) are seen. At the peak of the blooms the average cross-correlation values are very low due to the existence of blooms in both cyclones and anticyclones. The months after the winter and summer blooms show a clear difference in the correlations. After the winter bloom (typically April and May), the cross-correlation is positive or very small, which suggests no relation between the mesoscale eddies, and the blooms. As discussed in Kumar et al. (2001), low primary production is observed after termination of winter cooling during Spring Inter-Mansoon (SIM) (Gomes et al., 2008). This result would be also consistent with SIM producing weak atmospheric forcing in the region.

In contrast, after the summer bloom (typically October–December) as the average values of chlorophyll a decrease, chlorophyll and SSHA become relatively highly anti-correlated. The reason for the anti-correlation is the persistence of chlorophyll at the regions with negative SSHA that typically considered to be cyclonic (cold) eddies and disappearance of chlorophyll a in positive SSHA that assumed to be anti-cyclonic (warm) eddies. Particle backscatter also provides almost same cross-correlation and average

Blooms in the Northwestern Arabian Sea and Gulf of Oman

S. Sedigh Marvasti et al.

Title Page

Abstract   Introduction

Conclusions   References

Tables   Figures

◀   ▶

◀   ▶

Back   Close

Full Screen / Esc

Printer-friendly Version

Interactive Discussion

value results suggesting that the chlorophyll *a* signal does not result purely from photo-adaptation. Moreover, the CDOM-SSHA cross-correlation shows the same patterns for bloom times but typically shows lower correlation.

4 Numerical modelling results

4.1 Temporal variability

Annual cycles of variation of chlorophyll *a* and biomass for all GFDL models are shown in Fig. 7a, b within the whole region and compared against the corresponding GSM5 satellite results. Note that the 8 consequent years of the model output, selected as the last eight years of the run, would not be expected to correspond to the 8 actual years in the satellite data. The annual cycles of chlorophyll *a* and biomass are quite similar to each other in all GFDL models, insofar as they show two distinct blooms in yearly cycle. The maximum values that can be considered as a winter bloom in the whole region are mostly seen around February (Piontkovski et al., 2011), with values of 0.32–0.38, 0.48–0.62, 1.2 mg m^{-3} for chlorophyll and 31, 66, 100–120 mg C m^{-3} for biomass in CORE-TOPAZ, Coupled-TOPAZ, and CM2.6 (miniBLING), respectively. A summer bloom is also pronounced in September as a second maximum in the yearly cycle over the whole region, with peak magnitudes of about 0.52, 0.66, 0.8 mg m^{-3} for chlorophyll and 33, 59, 40 mg C m^{-3} for biomass, in CORE-TOPAZ, Coupled-TOPAZ, and CM2.6, respectively. Both chlorophyll *a* and carbon biomass show minimal values of 0.2 mg m^{-3}, and 10–20 mg C m^{-3}, respectively, in a yearly cycle over the whole region. Comparing the results of GFDL models against the satellite data shows that chlorophyll *a* prediction of the models is similar to the satellite observation data in terms of the minimum values and the timing of the summer and winter bloom. The CORE-TOPAZ and Coupled TOPAZ correctly simulate the summer bloom as being stronger than the winter bloom. However, in CM2.6 (miniBLING), the winter bloom in the region is stronger than the summer bloom.

Qualitatively speaking, both satellite data and CM2.6 (miniBLING) outputs show pronounced interannual variability in all measured parameters, while interannual variability of TOPAZ models is not large, as shown in Fig. 7. Due to the low resolution and also low interannual variability of the TOPAZ models we focus on variability within CM2.6 (miniBLING).

In the satellite data the summertime biomass ranges from $\sim 40\,\mathrm{mg\,C\,m^{-3}}$ in 2000 to $90\,\mathrm{mg\,C\,m^{-3}}$ in 2001, with a similar range of variation in chlorophyll from 1 to $2\,\mathrm{mg\,m^{-3}}$. In CM2.6 the summertime biomass ranges from 30 to $50\,\mathrm{mg\,C\,m^{-3}}$, a somewhat smaller relative range. The wintertime biomass ranges from ~ 30–$45\,\mathrm{mg\,C\,m^{-3}}$ in the satellite estimates but from 80 to 140 in the model, a somewhat larger relative range.

To study the mechanisms driving the blooms in the model, the biomass (mol P kg^{-1}) is compared with the light intensity in the mixed layer and the light-saturated photosynthesis rate (carbon specific) (s^{-1}) in Figs. 8a and b for January of year 195. The biomass production and mixed layer light intensity (Fig. 8a) are not meaningfully correlated parameters. On the other hand, the biomass and the light-saturated carbon specific growth rate (Fig. 8b; indicating the degree of nutrient limitation) are positively correlated. From this, it can be concluded that the blooms in this region are more driven by nutrient rather than light, consistent with, for example, Gomes et al. (2008).

The model saves out the individual tendency terms associated with advection, vertical diffusion and subgridscale eddy fluxes and time rate of change. For simplicity, in this paper we combine the vertical diffusive flux associated with small-scale mixing with that due to the mixed layer parameterization. Figure 9 shows the advection, diffusion and tendency flux terms for the whole region (56–66° E, 15–26° N) over a typical year. The results show that the dominant source in whole region during the winter bloom is diffusion, suggesting the model predicts excessively strong mixing during the wintertime. However the advection dominates diffusion in summer bloom in supplying the nutrients particularly during the months of July and August. The fact that the summertime bloom

Full Screen / Esc

is close to observations suggests that the model correctly simulates this wind-driven upwelling.

4.2 Blooms and sea surface height in CM2.6

4.2.1 Large-scale correlation

The relationship between SSHA and chlorophyll is quite different in the model as compared to the satellite. Monthly variation in the cross-correlation of chlorophyll and SSHA for 8 consequent years in CM2.6 is shown in Fig. 10. As in the remote sensing, the model shows annual cycles of variation in the cross-correlation, suggesting a repeatable yearly phenomenon in the region. However the structure of this annual cycle is not consistent with the satellite data. The model predicts several months (i.e. March–August) with anti-correlation for most of the years, but with values less than 0.5, smaller than the peak anti-correlation values in satellite results. The model also predicts that several other months (i.e. October–February) should have no or even positive correlation, while the satellite shows strong negative correlations during these months.

4.2.2 Blooms in mesoscale structures

Why does the GFDL CM2.6 model not produce the same relationship between SSHA and chlorophyll as the satellite? We can gain some insight by examining snapshots of the two fields. In Fig. 11a and b, sea surface chlorophyll *a* concentration and sea surface height anomaly (SSHA) are shown at two snapshots of time, 9 November and 28 December for model year 195. Comparing the figures with the corresponding satellite results in Fig. 3k and l, we see that the southern part of the GFDL model is more similar to the satellite data, with high concentrations of chlorophyll *a* tending to be located at the center of cyclones. In contrast, in the northern part of the region, the GFDL model predicts high chlorophyll at the edges of the cyclones as well as in the center of anticyclones. The eddy structures have smaller diameters in GFDL results

Full Screen / Esc

Printer-friendly Version

Interactive Discussion

than the field observations, though it is not clear whether this represents smoothing in the AVISO product or some physical weakness of the model.

We now focus on the few examples in our model output where chlorophyll blooms are found in the center of cyclonic eddies. These are denoted as E1 and E2 in Fig. 11a and b. To track the movement of the selected eddies, E1 and E2, over the time from 9 November to 28 December, modeled chlorophyll and SSHA are shown in Fig. 11c and d along two different latitudes, 16° N (for E1) and 19° N (for E2). Figure 11c shows that E1 moved westward during this period of time, and that the chlorophyll concentration was kept high within the central part of the eddy. E1 appears to be created by the passage of a cyclone, similar to the eddy observed by Wang and Zhao (2008) in the aftermath of Cyclone Gonu. Similarly, as shown in Fig. 11d, E2 was a persistent eddy with both central and edge blooms during the month of November that started to move towards the west during the December along 19° N. However, at other latitudes, the largest blooms offshore are found along gradients in SSH rather than being associated with maxima or minima. This suggests a different mechanism for producing blooms in the model. In particular eddies are known to be able to strip chlorophyll off the coastal regions. In some cases this can bring a chlorophyll plume from the edge to the interior part of the eddy (Abbott and Zion, 1985; Giddings et al., 2014). Satellite data (i.e. see Fig. 3e) provide some hints for the existence of advective chlorophyll plumes being advected away from coastal regions. As shown in Fig. 11a and b, high velocities in the marginal region between adjacent cyclonic and anticyclonic eddies can cause such plumes in the GFDL models as well.

Why is the model only able to simulate the relationship between SSH and chlorophyll in the southern part of the domain? We hypothesize this is due to differences in stratification between the two regions. The average water temperature (colors) and the macronutrient (PO_4) concentrations (contours) for model year 197 are compared to the corresponding measured values in World Ocean Atlas (WOA09) within the upper 200 m in the northern (60–66° E and 19–23° N) and southern (60–66° E and 15–17° N) part of the region are shown in Fig. 12. In the northern part of the region (see Fig. 12a and

b), the GFDL model provides a reasonably good estimation of the mean temperature field near the surface, but subsurface temperatures are not as consistent as there is far too little stratification. This is also associated with a very weak nutricline in CM2.6. Variations in isopycnal depth will therefore not lead to big differences in nutrient supply.

⁵ Figures 12c and d show the same results for the southern part of the region. Unlike the northern part of the domain, the temperature gradient over these depths is well estimated by CM2.6. While the nutricline is still too weak there is some gradient in nutrients between 80 and 120 m.

A hypothesis for why we have too much warm water in the northern part of the

¹⁰ Arabian Sea is that too much water from Persian Gulf is found in this region. This can be seen in the yearly averaged subsurface salinity-density distribution over the region, shown in Fig. 12e and f for both WOA09 data and CM2.6 (model year 197), respectively. Figure 12e shows two separate tongues of salty water, one near the surface and one at the depth of ∼ 300 m. These salty water signals are consistent with the seasonal cycle

¹⁵ of Persian Gulf outflow as discussed in Ezam et al. (2010). On the other hand, CM2.6 shows one subsurface salty water signal from the northern part, which is deep and strong enough to result in weak stratification in the north to a depth of 250 m, as shown in Fig. 12f. These results suggest that a sharp thermocline and nutricline is necessary for eddy activity to modulate the mixing of nutrients to the surface.

²⁰ We test the idea that a sharper thermocline could modulate mixing of nutrients to the surface by looking at the sources of nutrient in the southern part of Arabian Sea where eddy-bloom relationships are seen. Accordingly, the region containing eddy E1 in Fig. 11 is analyzed to determine the physical mechanisms by which nutrient is transported into the surface layer. Figure 13 contrasts chlorophyll concentration, advection,

²⁵ and diffusion terms for the region from 63–66° E, 15–18° N over the December of two consecutive CM2.6 years of 197 and 198. In Year 197 we see an eddy associated with a bloom while there is no eddy in year 198 at the same time and the chlorophyll concentrations are much lower. In both years the diffusive flux of nutrient to the top 50 m mirrors the chlorophyll. But in 197 it is larger and positive ($\sim 10\,\mathrm{mol\,m^{-2}\,month^{-1}}$) in the

Full Screen / Esc

Printer-friendly Version

Interactive Discussion

eddy while the advective flux is actually negative in this region. By contrast in Year 198, there is no cyclonic eddy and the diffusive fluxes are much smaller.

To summarize, we hypothesize that.

1. The reason that blooms are found in cyclones in the Arabian Sea during the NEM is that the dominant source of nutrients to the surface, i.e. mixing (Barimalala et al., 2013; Kawamiya and Oschlies, 2003) is concentrated there.

2. Interannual variability in wintertime blooms in the Northwest Arabian Sea is controlled by the combined presence of these eddies and strength of wintertime cooling.

3. Excessive mixing (resulting in too weak a thermocline) prevents mixing from being modulated by eddies in the model except occasionally in the southern part of our region. In the real world the modulation of mixing seen in Fig. 13 extends into the Northwest Arabian Sea and the Gulf of Oman.

5 Conclusions

Our analysis of bloom variability in the northwestern Arabian Sea and Gulf of Oman has illustrated a set of both similar and dissimilar descriptive features between satellites and among a suite of models and explored the various mechanisms involved. Satellite analyses verified the existence of two blooms, the stronger one associated with the Southwest monsoon and the weaker one associated with the Northeast Monsoon as also shown by Madhupratap et al. (1996), Kawamiya and Oschlies (2003), Murtugudde et al. (2007), and Al-Azri et al. (2010). We demonstrate a pronounced anti-correlation between SSHA and chlorophyll blooms in during certain times in northern winter but a much weaker relationship in other months (typically northern summer) with the blooms going away in the months of April and May (northern spring). While the depth of thermocline and nutricline and also stratification are affecting the convection

during the Northeast Monsoon (Dickey et al., 1998; Kumar et al., 2001; Wiggert et al., 2002), we show that a thin nutricline/thermocline and a strong stratification are also required to enable cold eddies to bring nutrients to euophotic zone and develop phytoplankton blooms. During the wintertime monsoon, while both cooling in the winter and
5 eddies control the blooms, variability in bloom location will arise from variability in the location of eddies, and so may not be predictable. In contrast, during the Southwest Monsoon the dominant upwelling associated with the intense environmental forcing supersedes the effect of eddies and the activity of the cold eddies is not pronounced.

Understanding of this phenomenon has been sought using three different 3-D
10 ocean–atmosphere models, including a CORE-forced ocean with the TOPAZ biogeochemistry, a coupled model with the TOPAZ biogeochemisty and CM2.6. Because the coarse models with TOPAZ are not able to capture eddies and the interannual variability, CM2.6 (miniBLING), a eddy-resolving high resolution model, was also considered for simulating the spatial and temporal changes of the bloom in the region. This model
15 simulates the two blooms seen in the data and shows that the nutrients driving the northern summer bloom are supplied by advection while those driving the wintertime bloom are supplied by vertical diffusion. However, this model is unable to simulate the seasonal relationship observed in the satellite products between blooms and sea surface height. Although there is some anti-correlation, it tends to be associated with
20 larger spatial scales and not really related to eddies. Instead, eddies in the model usually wrap the chlorophyll around themselves, producing high chlorophyll concentrations around their edges and not at their centers. Comparing the model results to field measurements (WOA09) showed that the model does not account for the strong thermocline and nutricline in the northern part of the region. In the wintertime, this leads to
25 excessive convective supply of nutrients and too strong of a bloom. However, for a few cases eddies with a bloom at the center are tracked in the southern part of the domain. In this region consistency is observed between the model results and the field data. Analysis of the term balances in mixed layer show that eddies in this region modulate the diffusive supply of nutrients. We suggest that what happens in the model in the

Southern Arabian Sea actually describes the Arabian Sea as a whole according to the observations and the field data. The model misses the eddy signal in the north because it lacks a thin nutricline, motions of which will lead to differences in nutrient supply. In the real world, eddies modulate the diffusive supply of nutrients during the wintertime and there is more mixing in the eddy centers along with the diffusive supply provided by the cooling in the wintertime. Accordingly, there is a potential to improve the numerical models by better simulating the Persian Gulf Outflow to produce a sharper thermocline, allowing more realistic nutrient supply.

References

Abbott, M. R. and Zion, P. M.: Satellite observations of phytoplankton variability during an upwelling event, Cont. Shelf Res., 4, 661–680, doi:10.1016/0278-4343(85)90035-4, 1985.

Adcroft, A., Campin, J.-M., Hill, C., and Marshall, J.: Implementation of an atmosphere–ocean general circulation model on the expanded spherical cube, Mon. Weather Rev., 132, 2845–2863, doi:10.1175/MWR2823.1, 2004.

Al-Azri, A. R., Piontkovski, S. A., Al-Hashmi, K. A., Goes, J. I., and Gomes, H. R.: Chlorophyll *a* as a measure of seasonal coupling between phytoplankton and the monsoon periods in the Gulf of Oman, Aquat. Ecol., 44, 449–461, doi:10.1007/s10452-009-9303-2, 2010.

Al-Azri, A. R., Piontkovski, S. A., Al-Hashmi, K. A., Goes, J. I., Gomes, H. D. R., and Glibert, P. M.: Mesoscale and nutrient conditions associated with the massive 2008 cochlodinium polykrikoides bloom in the Sea of Oman/Arabian Gulf, Estuar. Coast., 37, 325–338, doi:10.1007/s12237-013-9693-1, 2013.

Anderson, D. M. and Prell, W. L.: A 300 KYR Record of Upwelling Off Oman During the Late Quaternary: evidence of the Asian Southwest Mansoon, Paleoceanography, 8, 193–208, 1993.

Armstrong, R. A., Lee, C., Hedges, J. I., Honjo, S., and Wakeham, S. G.: A new, mechanistic model for organic carbon fluxes in the ocean based on the quantitative associa-

Blooms in the Northwestern Arabian Sea and Gulf of Oman

S. Sedigh Marvasti et al.

tion of POC with ballast minerals, Deep-Sea Res. Pt. II, 49, 219–236, doi:10.1016/S0967-0645(01)00101-1, 2002.

Banse, K. and English, D. C.: Revision of satellite-based phytoplankton pigment data from the Arabian Sea during the Northeast Monsoon, Mar. Res., 2, 83–103, 1993.

5 Banse, K. and McClain, C. R.: Winter blooms of phytoplankton in the Arabian Sea as observed by the Coastal Zone Color Scanner, Mar Ecol Prog Ser, 34, 201–211, 1986.

Barimalala, R., Bracco, A., Kucharski, F., McCreary, J. P., and Crise, A.: Arabian Sea ecosystem responses to the South Tropical Atlantic teleconnection, J. Marine Syst., 117–118, 14–30, doi:10.1016/j.jmarsys.2013.03.002, 2013.

10 Bartolacci, D. M. and Luther, M. E.: Patterns of co-variability between physical and biological parameters in the Arabian Sea, Deep-Sea Res. Pt. II, 46, 1933–1964, doi:10.1016/S0967-0645(99)00049-1, 1999.

Behrenfeld, M., Boss, E., Siegel, D. A., and Shea, D. M.: Carbon-based ocean productivity and phytoplankton physiology from space, Global Biogechem. Cy., 19, 1,
15 doi:10.1029/2004GB002299, 2005.

Bryan, K. and Lewis, L. J.: A water mass moel of the world ocean, J. Geophys. Res.-Oceans, 84, 2503–2517, 1979.

Danabasoglu, G., Large, W. G., Tribbia, J. J., Gent, P. R., Briegleb, B. P., and McWilliams, J. C.: Diurnal coupling in the tropical oceans of CCSM3, J. Climate, 19, 2347–
20 2365, doi:10.1175/JCLI3739.1, 2006.

Delworth, T. L., Broccoli, A. J., Rosati, A., Stouffer, R. J., Balaji, V., Beesley, J. A., Cooke, W. F., Dixon, K. W., Dunne, J., Dunne, K. A., Durachta, J. W., Findell, K. L., Ginoux, P., Gnanade-sikan, A., Gordon, C. T., Griffies, S. M., Gudgel, R., Harrison, M. J., Held, I. M., Hem-ler, R. S., Horowitz, L. W., Klein, S. A., Knutson, T. R., Kushner, P. J., Langenhorst, A. R.,
25 Lee, H. C., Lin, S. J., Lu, J., Malyshev, S. L., Milly, P. C. D., Ramaswamy, V., Russell, J., Schwarzkopf, M. D., Shevliakova, E., Sirutis, J. J., Spelman, M. J., Stern, W. F., Winton, M., Wittenberg, A. T., Wyman, B., Zeng, F., and Zhang, R.: GFDL's CM2 global coupled cli-mate models. Part I: Formulation and simulation characteristics, J. Climate, 19, 643–674, doi:10.1175/JCLI3629.1, 2006.

30 Delworth, T. L., Rosati, A., Anderson, W., Adcroft, A. J., Balaji, V., Benson, R., Dixon, K., Griffies, S. M., Lee, H.-C., Pacanowski, R. C., Vecchi, G. A., Wittenberg, A. T., Zeng, F., and Zhang, R.: Simulated climate and climate change in the GFDL CM2.5 high-resolution coupled climate model, J. Climate, 25, 2755–2781, doi:10.1175/JCLI-D-11-00316.1, 2012.

Dickey, T., Marra, J., Sigurdson, D. E., Weller, R. A., Kinkade, C. S., Zedler, S. E., Wiggert, J. D., and Langdon, C.: Seasonal variability of bio-optical and physical properties in the Arabian Sea?: October 1994–October 1995, Deep-Sea Res. Pt. II, 45, 2001–2025, 1998.

Dunne, J. P., Sarmiento, J. L., and Gnanadesikan, A.: A synthesis of global particle export from the surface ocean and cycling through the ocean interior and on the seafloor, Global Biogeochem. Cy., 21, 1–16, doi:10.1029/2006GB002907, 2007.

Dunne, J. P., John, J. G., Adcroft, A. J., Griffies, S. M., and Hallberg, R. W.: GFDL's ESM2 global coupled climate-carbon earth system models. Part I: physical formulation and baseline simulation characteristics, J. Climate, 25, 6646–6665, doi:10.1175/JCLI-D-11-00560.1, 2012.

Dunne, J. P., John, J. G., Shevliakova, S., Stouffer, R. J., Krasting, J. P., Malyshev, S. L., Milly, P. C. D., Sentman, L. T., Adcroft, A. J., Cooke, W., Dunne, K. A., Griffies, S. M., Hallberg, R. W., Harrison, M. J., Levy, H., Wittenberg, A. T., Phillips, P. J., and Zadeh, N.: GFDL's ESM2 global coupled climate-carbon earth system models. Part II: Carbon system formulation and baseline simulation characteristics, J. Climate, 26, 2247–2267, doi:10.1175/JCLI-D-12-00150.1, 2013.

Eden, B. R., Steinberg, D. K., Goldthwait, S. A., and McGillicuddy, D. J.: Zooplankton community structure in a cyclonic and mode-water eddy in the Sargasso Sea, Deep-Sea Res. Pt. I, 56, 1757–1776, doi:10.1016/j.dsr.2009.05.005, 2009.

Ewart, C. S., Meyers, M. K., Wallner, E. R., McGillicuddy, D. J., and Carlson, C. A.: Microbial dynamics in cyclonic and anticyclonic mode-water eddies in the northwestern Sargasso Sea, Deep-Sea Res. Pt. II, 55, 1334–1347, doi:10.1016/j.dsr2.2008.02.013, 2008.

Ezam, M., Bidokhti, A. A., and Javid, A. H.: Numerical simulations of spreading of the Persian Gulf outflow into the Oman Sea, Ocean Sci., 6, 887–900, doi:10.5194/os-6-887-2010, 2010.

Fatemi, S., Nabavi, S., Vosoghi, G., Fallahi, M., and Mohammadi, M.: The relation between environmental parameters of Hormuzgan coastline in Persian Gulf and occurrence of the first harmful algal bloom of Cochlodinium polykrikoides, Iran. J. Fish. Sci., 11, 475–489, 2012.

Fischer, A. S., Weller, R. A., Rudnick, D. L., Eriksen, C. C., Lee, C. M., Brink, K. H., Fox, C. A., and Leben, R. R.: Mesoscale eddies, coastal upwelling, and the upper-ocean heat budget in the Arabian Sea, Deep-Sea Res. Pt. II, 49, 2231–2264, doi:10.1016/S0967-0645(02)00036-X, 2002.

Fox-Kemper, B., Ferrari, R., and Hallberg, R.: Parameterization of mixed layer eddies. Part I: theory and diagnosis, J. Phys. Oceanogr., 38, 1145–1165, doi:10.1175/2007JPO3792.1, 2008.

Galbraith, E. D., Gnanadesikan, A., Dunne, J. P., and Hiscock, M. R.: Regional impacts of iron-light colimitation in a global biogeochemical model, Biogeosciences, 7, 1043–1064, doi:10.5194/bg-7-1043-2010, 2010.

Galbraith, E. D., Dunne, J. P., Gnanadesikan, A., Richard, D., Sarmiento, J. L., Dufour, C. O., Gregory, F., Bianchi, D., Claret, M., Rodgers, K. B., and Sedigh Marvasti, S.: Parameterized complexity for simulating realistic biogeochemistry with few tracers in Earth System Models, J. Adv. Model. Earth Syst., in review, 2015.

Giddings, S. N., MacCready, P., Hickey, B. M., Banas, N. S., Davis, K. A., Siedlecki, S. A., Trainer, V. L., Kudela, R. M., Pelland, N. A., and Connolly, T. P.: Hindcasts of potential harmful algal bloom transport pathways on the Pacific Northwest coast, J. Geophys. Res.-Oceans, 119, 2439–2461, 2014.

Gnanadesikan, A., Dixon, K. W., Griffies, S. M., Balaji, V., Barreiro, M., Beesley, J. A., Cooke, W. F., Delworth, T. L., Gerdes, R., Harrison, M. J., Held, I. M., Hurlin, W. J., Lee, H. C., Liang, Z., Nong, G., Pacanowski, R. C., Rosati, A., Russell, J., Samuels, B. L., Song, Q., Spelman, M. J., Stouffer, R. J., Sweeney, C. O., Vecchi, G., Winton, M., Wittenberg, A. T., Zeng, F., Zhang, R., and Dunne, J. P.: GFDL's CM2 global coupled climate models. Part II: The baseline ocean simulation, J. Climate, 19, 675–697, doi:10.1175/JCLI3630.1, 2006.

Gnanadesikan, A., Dunne, J. P., and John, J.: What ocean biogeochemical models can tell us about bottom-up control of ecosystem variability, ICES J. Mar. Sci., 68, 1030–1044, doi:10.1093/icesjms/fsr068, 2011.

Gnanadesikan, A., Dunne, J. P., and Msadek, R.: Connecting Atlantic temperature variability and biological cycling in two earth system models, J. Marine Syst., 133, 39–54, doi:10.1016/j.jmarsys.2013.10.003, 2014.

Gomes, R., Goes, J. I., Matondkar, S. G. P., Parab, S. G., Al-azri, A. R. N., and Thoppil, P. G.: Deep-Sea Research I Blooms of Noctiluca miliaris in the Arabian Sea – An in situ and satellite study, Deep-Sea Res. Pt. I, 55, 751–765, doi:10.1016/j.dsr.2008.03.003, 2008.

Griffies, S. M., Gnanadesikan, A., Dixon, K. W., Dunne, J. P., Gerdes, R., Harrison, M. J., Rosati, A., Russell, J. L., Samuels, B. L., Spelman, M. J., Winton, M., and Zhang, R.: Formulation of an ocean model for global climate simulations, Ocean Sci., 1, 45–79, doi:10.5194/os-1-45-2005, 2005.

Blooms in the Northwestern Arabian Sea and Gulf of Oman

S. Sedigh Marvasti et al.

Title Page

Abstract	Introduction
Conclusions	References
Tables	Figures

|◄ | ►|

◄ | ►

Back | Close

Full Screen / Esc

Printer-friendly Version

Interactive Discussion

Griffies, S. M., Biastoch, A., Böning, C., Bryan, F., Danabasoglu, G., Chassignet, E. P., England, M. H., Gerdes, R., Haak, H., Hallberg, R. W., Hazeleger, W., Jungclaus, J., Large, W. G., Madec, G., Pirani, A., Samuels, B. L., Scheinert, M., Gupta, A. S., Severijns, C. A., Simmons, H. L., Treguier, A. M., Winton, M., Yeager, S., and Yin, J.: Coordinated Ocean-ice Reference Experiments (COREs), Ocean Model., 26, 1–46, doi:10.1016/j.ocemod.2008.08.007, 2009.

Hamzehei, S., Bidokhti, A. A., Seddiq Mortazavi, M., and Gheiby, A.: Red Tide Monitoring in the Persian Gulf and Gulf of Oman Using MODIS Sensor Data, Tech. J. Eng. Appl. Sci., 3, 1100–1107, 2013.

Hamzehei, S., Bidokhti, A., Mortazavi, M. S., Gheiby, A., Ebrahimi, M., and Saraji, F.: Field study of the 2008–2009 red tide in the northern Strait of Hormuz, Life Sci. J., 9, 4727–4733, 2012.

Honjo, S., Dymond, J., Prell, W., and Ittekkot, V.: Monsoon-controlled export fluxes to the interior of the Arabian Sea, Deep-Sea Res. Pt. II, 46, 1859–1902, 2000.

Kawamiya, M. and Oschlies, A.: An eddy-permitting, coupled ecosystem-circulation model of the Arabian Sea?: comparison with observations, J. Marine Syst., 38, 221–257, 2003.

Klaas, C. and Archer, D. E.: Association of sinking organic matter with various types of mineral ballast in the deep sea: implications for the rain ratio, Global Biogeochem. Cy., 16, 1116, doi:10.1029/2001GB001765, 2002.

Kumar, S. P., Ramaiah, N., Gauns, M., Sarma, V. V. S. S., Muraleedharan, P. M., Raghukumar, S., Kumar, M. D., and Madhupratap, M.: Physical forcing of biological productivity in the Northern Arabian Sea during the Northeast Monsoon, Deep-Sea Res. Pt. II, 48, 1115–1126, 2001.

Large, W. G., McWilliams, J. C., and Doney, S. C.: Oceanic vertical mixing: a review and a model with a nonlocal boundary layer parameterization, Rev. Geophys., 32, 363, doi:10.1029/94RG01872, 1994.

Lee, M.-M. and Williams, R. G.: The role of eddies in the isopycnic transfer of nutrients and their impact on biological production, J. Mar. Res., 58, 895–917, doi:10.1357/002224000763485746, 2000.

Lee, M.-M., Nurser, A. J. G., Coward, A. C., and de Cuevas, B. A.: Eddy advective and diffusive transports of heat and salt in the Southern Ocean, J. Phys. Oceanogr., 37, 1376–1393, doi:10.1175/JPO3057.1, 2007.

Title Page

Abstract | Introduction

Conclusions | References

Tables | Figures

◄ | ►

◄ | ►

Back | Close

Full Screen / Esc

Printer-friendly Version

Interactive Discussion

Levy, M., Memery, L., and Madec, G.: The onset of a bloom after deep winter convection in the northwestern Mediterranean sea: mesoscale process study with a primitive equation model, J. Marine Syst., 16, 7–21, 1998.

Levy, M., Shankar, D., Andre, J., Shenoi, S. S. C., Durand, F., and Montegut, C. D. B.: Basin-wide seasonal evolution of the Indian Ocean's phytoplankton blooms, J. Geophys. Res., 112, 1–14, 2007.

Madhupratap, M., Kumar, S., Bhattathiri, P., Kumar, M., Raghukumar, S., Nair, K., and Rama-iah, N.: Mechanism of the biological response to winter cooling in the northeastern Arabian Sea, Nature, 384, 549–552, 1996.

Maritorena, S., Siegel, D. A., and Peterson, A. R.: Optimization of a semianalytical ocean color model for global-scale applications, Appl. Optics, 41, 2705–2714, 2002.

McGillicuddy, D. J., Robinson, A. R., Siege, D. A., Jannasch, H. W., Johnsonk, R., Dickey, T. D., McNeil, J., Michaels, A. F., and Knapk, A. H.: Influence of mesoscale eddies on new production in the Sargasso Sea, Nature, 285, 263–266, 1998.

McGillicuddy, D. J., Johnson, R., Siegel, D. A., Michaels, A. F., Bates, N. R., and Knap, A. H.: Mesoscale variations of biogeochemical properties in the Sargasso Sea, J. Geophys. Res., 104, 381–394, 1999.

McGillicuddy, D., Kosnyrev, V., Ryan, J., and Yoder, J.: Covariation of mesoscale ocean color and sea-surface temperature patterns in the Sargasso Sea, Deep-Sea Res. Pt. II, 48, 1823–1836, 2001.

McGillicuddy, D. J., Anderson, L. A., Bates, N. R., Bibby, T., Buesseler, K. O., Carlson, C. A., Davis, C. S., Ewart, C., Falkowski, P. G., Goldthwait, S. A., Hansell, D. A., Jenkins, W. J., Johnson, R., Kosnyrev, V. K., Ledwell, J. R., Li, Q. P., Siegel, D. A., and Steinberg, D. K.: Eddy/wind interactions stimulate extraordinary mid-ocean plankton blooms, Science, 316, 1021–1026, doi:10.1126/science.1136256, 2007.

Murtugudde, R., Seager, R., and Thoppil, P.: Arabian Sea response to monsoon variations, Paleoceanography, 22, 1–17, doi:10.1029/2007PA001467, 2007.

Naqvi, S. W. A., Moffett, J. W., Gauns, M. U., Narvekar, P. V., Pratihary, A. K., Naik, H., Shenoy, D. M., Jayakumar, D. A., Goepfert, T. J., Patra, P. K., Al-Azri, A., and Ahmed, S. I.: The Arabian Sea as a high-nutrient, low-chlorophyll region during the late Southwest Monsoon, Biogeosciences, 7, 2091–2100, doi:10.5194/bg-7-2091-2010, 2010.

Nencioli, F., Dong, C., Dickey, T., Washburn, L., and Mcwilliams, J. C.: A vector geometry-based eddy detection algorithm and its application to a high-resolution numerical model product and

high-frequency radar surface velocities in the Southern California Bight, J. Atmos. Ocean. Tech., 27, 564–579, doi:10.1175/2009JTECHO725.1, 2010.

Piontkovski, S., Al-Azri, A., and Al-Hashmi, K.: Seasonal and interannual variability of chloro-phyll *a* in the Gulf of Oman compared to the open Arabian Sea regions, Int. J. Remote Sens., 32, 7703–7715, doi:10.1080/01431161.2010.527393, 2011.

Piontkovski, S., Al-Gheilani, H., Jupp, B., Al-Azri, A., and Al-hashmi, K.: Interannual changes in the Sea of Oman Ecosystem., Open Mar. Biol. J., 6, 38–52, 2012.

Richlen, M. L., Morton, S. L., Jamali, E. A., Rajan, A., and Anderson, D. M.: The catastrophic 2008–2009 red tide in the Arabian gulf region, with observations on the identification and phy-logeny of the fish-killing dinoflagellate Cochlodinium polykrikoides, Harmful Algae, 9, 163–172, doi:10.1016/j.hal.2009.08.013, 2010.

Sarmiento, J. L., Slater, R. D., Dunne, J., Gnanadesikan, A., and Hiscock, M. R.: Efficiency of small scale carbon mitigation by patch iron fertilization, Biogeosciences, 7, 3593–3624, doi:10.5194/bg-7-3593-2010, 2010.

Shalapyonok, A., Olson, R. J., and Shalapyonok, L. S.: Arabian Sea phytoplankton during Southwest and Northeast Monsoons 1995?: composition, size structure and biomass from individual cell properties measured by # ow cytometry, Deep-. Res. II, 48, 1231–1261, 2001.

Simmons, H. L., Jayne, S. R., St. Laurent, L. C., and Weaver, A. J.: Tidally driven mix-ing in a numerical model of the ocean general circulation, Ocean Model., 6, 245–263, doi:10.1016/S1463-5003(03)00011-8, 2004.

Stacey, M. W., Pond, S., and Nowak, Z. P.: A Numerical Model of the Circulation in Knight Inlet, British Columbia, Canada, J. Phys. Oceanogr., 25, 1037–1062, doi:10.1175/1520-0485(1995)025<1037:ANMOTC>2.0.CO;2, 1995.

Sweeney, E. N., McGillicuddy, D. J., and Buesseler, K. O.: Biogeochemical impacts due to mesoscale eddy activity in the Sargasso Sea as measured at the Bermuda Atlantic Time-series Study (BATS), Deep-Sea Res. Pt. II, 50, 3017–3039, doi:10.1016/j.dsr2.2003.07.008, 2003.

Tang, D., Kawamura, H., and Luis, A. J.: Short-term variability of phytoplankton blooms associ-ated with a cold eddy in the northwestern Arabian Sea, Remote Sens. Environ., 81, 82–89, 2002.

Veldhuis, M. J. W., Kraay, G. W., Van Bleijswijk, J. D. L., and Baars, M. A.: Seasonal and spa-tial variability in phytoplankton biomass, productivity and growth in the northwestern Indian

Ocean?: the southwest and northeast monsoon, 1992–1993, Deep-Sea Res. Pt. I, 44, 425–449, 1997.

Wang, D. and Zhao, H.: Estimation of phytoplankton responses to Hurricane Gonu over the Arabian Sea based on ocean color data, Sensors, 8, 4878–4893, doi:10.3390/s8084878, 2008.

Wiggert, J. D., Murtugudde, R. G., and Mcclain, C. R.: Processes controlling interannual variations in wintertime (Northeast Monsoon) primary productivity in the central Arabian Sea, Deep-Sea Res. Pt. II, 49, 2319–2343, 2002.

Wiggert, J. D., Murtugudde, R. G., and Christian, J. R.: Annual ecosystem variability in the tropical Indian Ocean?: results of a coupled bio-physical ocean general circulation model, Deep-Sea Res. Pt. II, 53, 644–676, doi:10.1016/j.dsr2.2006.01.027, 2006.
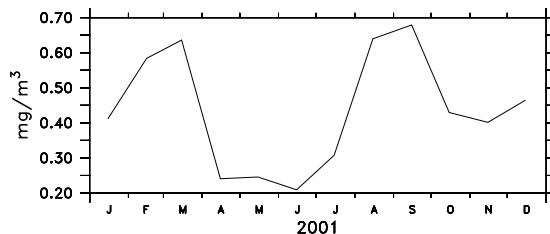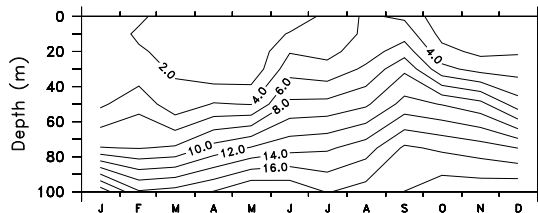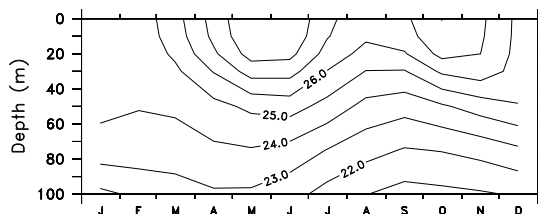
Figure 1. Monthly average for region from 56° E-66° E, 15° N-26° N: **(a)** surface chlorophyll *a* in 2001 (SeaWIFS); **(b)** nitrate (WOA09) over top 100 m; **(c)** temperature over top 100 m.
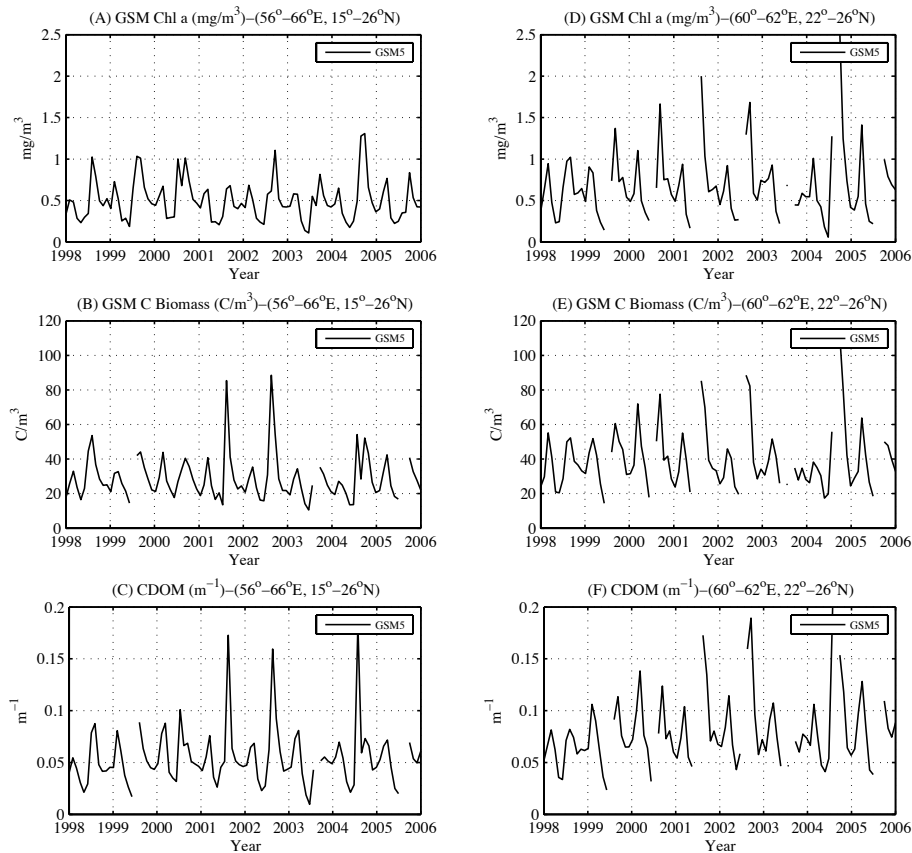
Figure 2. Monthly variation of organic matter in satellite data between 1998 and 2005 within 56–66° E, 15–26° N (large region); and 60–62° E, 22–26° N (small region): **(a)** and **(d)** chlorophyll; **(b)** and **(e)** particulate backscatter; **(c)** and **(f)** CDOM.
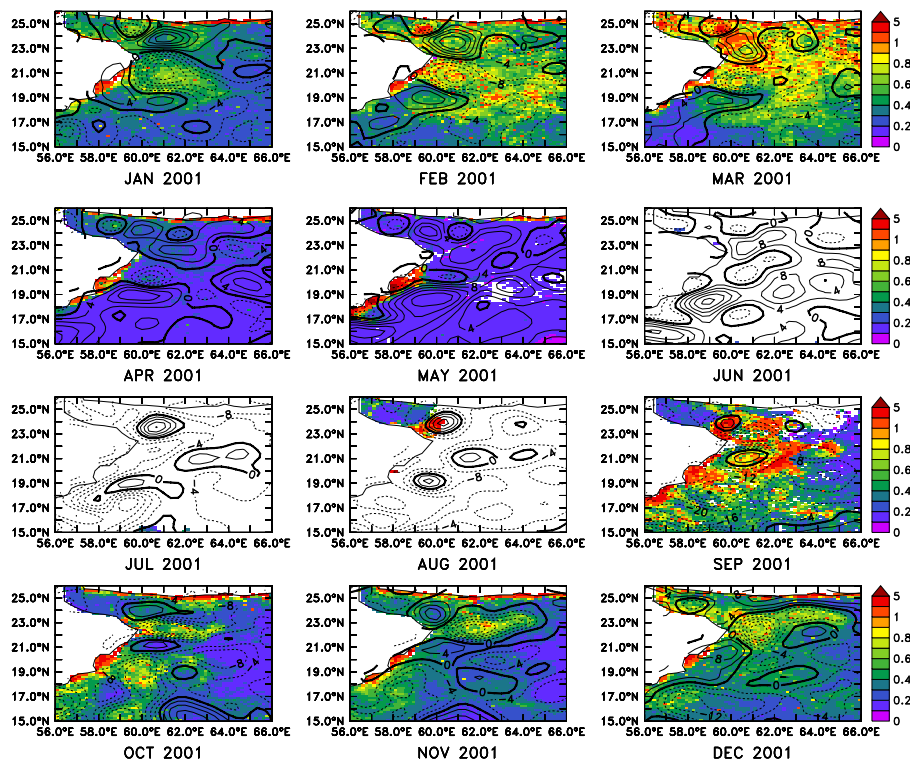
Figure 3. Chlorophyll *a* in mg m^{-3} (colors) and Sea-Surface height anomaly (SSHA, contours) in meter in Gulf of Oman in 2001.
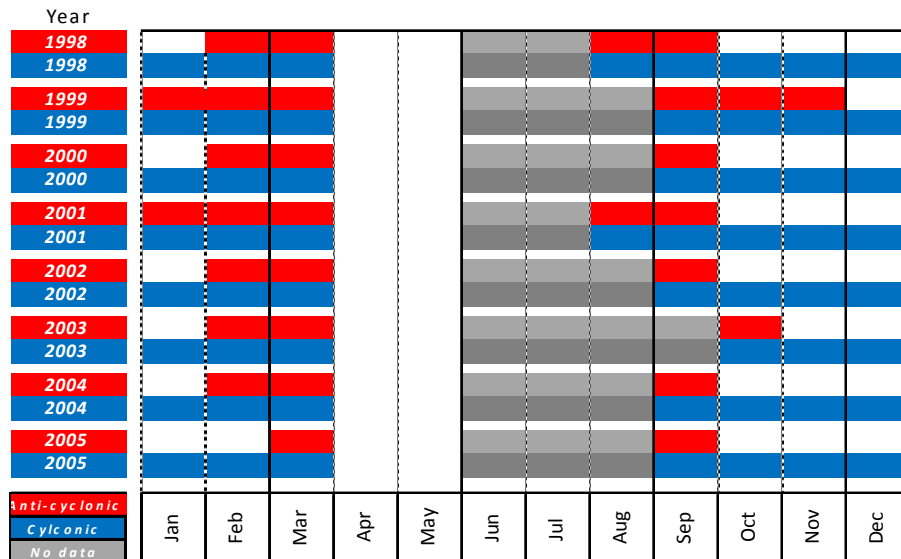
Figure 4. Qualitative eddy-chlorophyll *a* correlation in the Gulf of Oman (1998–2005).

Title Page

Abstract | Introduction

Conclusions | References

Tables | Figures

|◄ | ►|

◄ | ►

Back | Close

Full Screen / Esc

Printer-friendly Version

Interactive Discussion
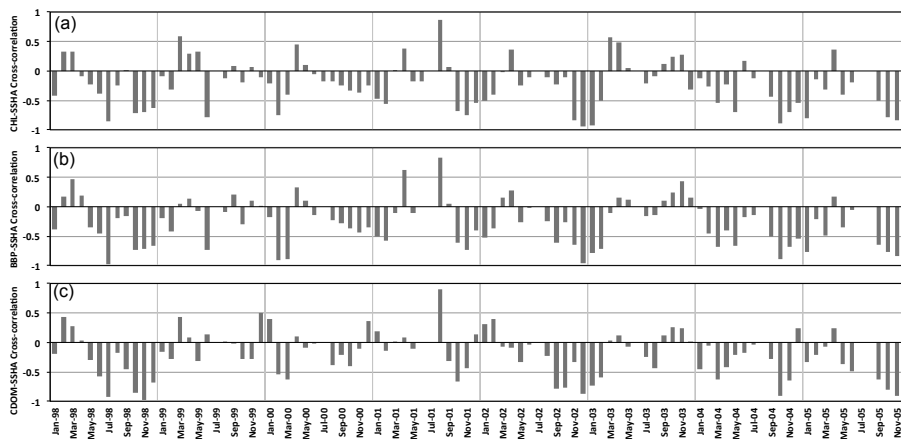
Figure 5. Monthly chlorophyll-SSHA cross-correlation between 1998 and 2005 within 56–66° E and 15–26° N. **(a)** chlorophyll; **(b)** BBP; **(c)** CDOM.
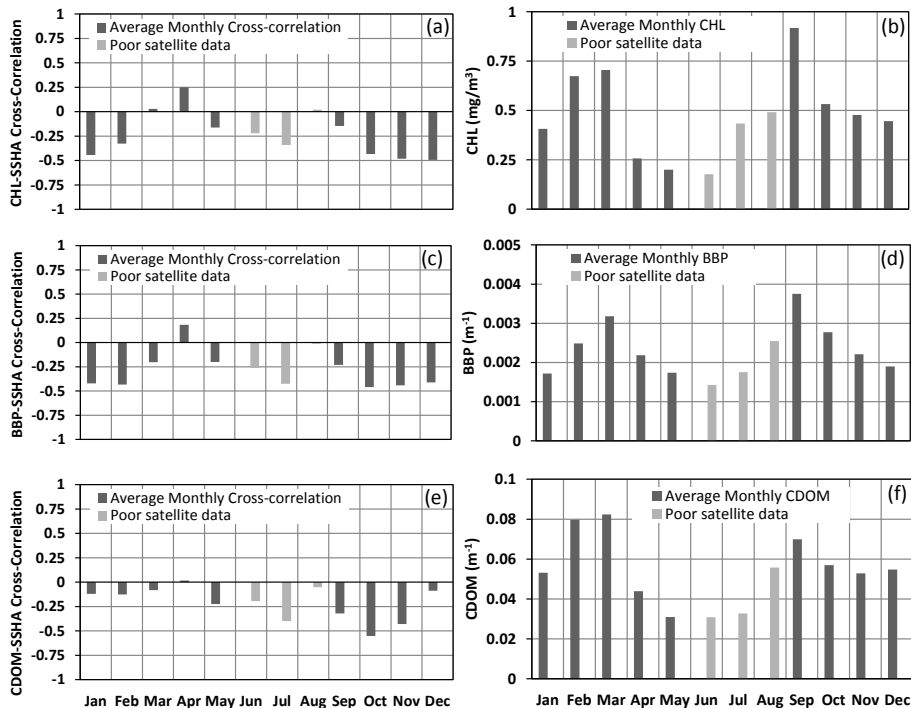
Figure 6. Average monthly cross-correlation with SSHA and average monthly values between 1998 and 2005 within 56–66° E and 15–26° N: **(a)**, **(b)** chlorophyll; **(c)**, **(d)** backscatter; **(e)**, **(f)** CDOM.

Title Page

Abstract | Introduction

Conclusions | References

Tables | Figures

◀◀ | ▶▶

◀ | ▶

Back | Close

Full Screen / Esc

Printer-friendly Version

Interactive Discussion
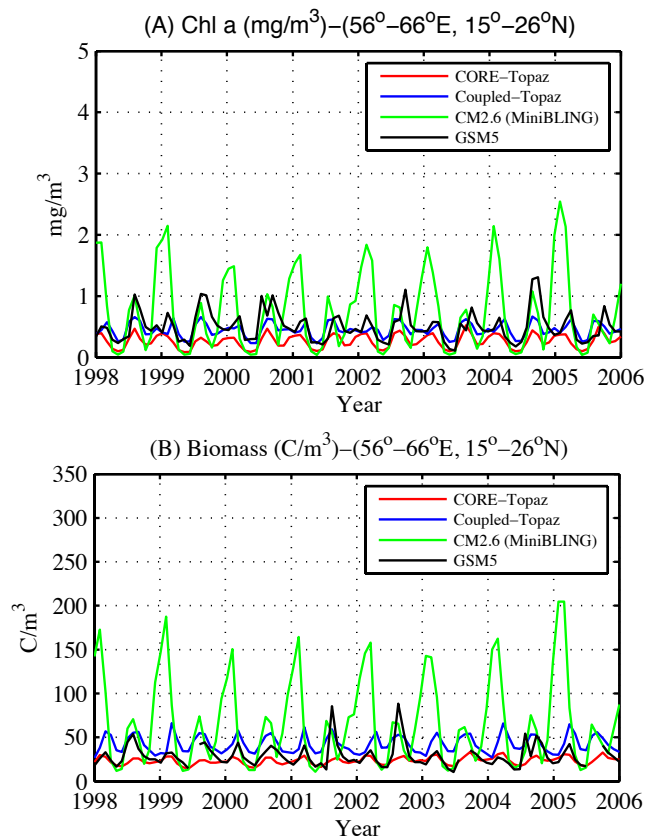
Figure 7. Monthly variation of organic matter in satellite data between 1998 and 2005 and GFDL models (8 characteristic years) within 56–66° E, 15–26° N: **(a)** chlorophyll from GFDL models and GSM5 algorithm; **(b)** carbon biomass from GFDL models and GSM5 algorithm.

Title Page

Abstract | Introduction

Conclusions | References

Tables | Figures

|◄ | ►|

◄ | ►

Back | Close

Full Screen / Esc

Printer-friendly Version

Interactive Discussion
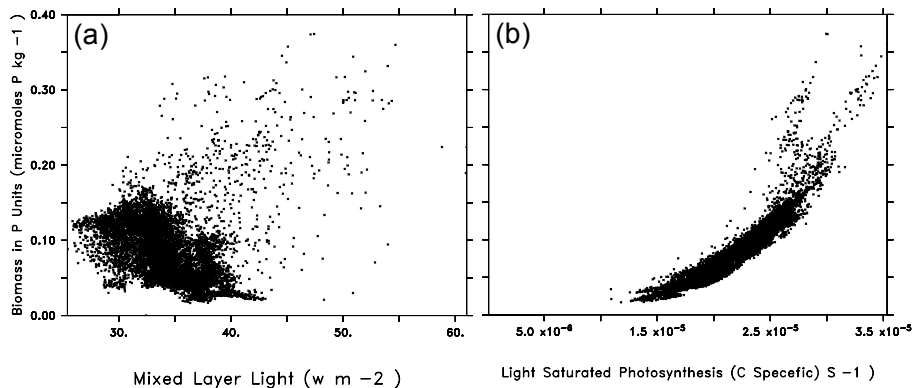
Figure 8. Modeled biomass in CM2.6 in P units (mol P kg^{-1}) vs.: **(a)** mixed layer irradiance (W m^{-2}); **(b)** light-saturated photosynthesis rate (carbon specific) (s^{-1}) 56–66° E, 15–26° N for January of year 195.
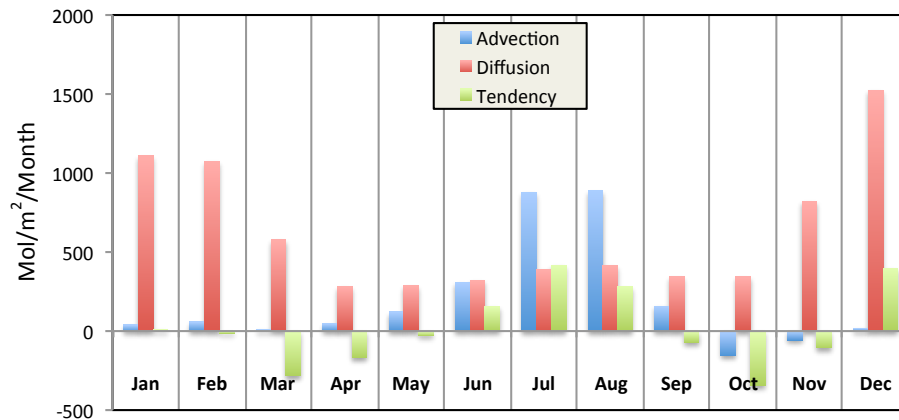
Figure 9. Advection, diffusion and tendency flux from the CM2.6 model over the whole region (56–66° E, 15–26° N).
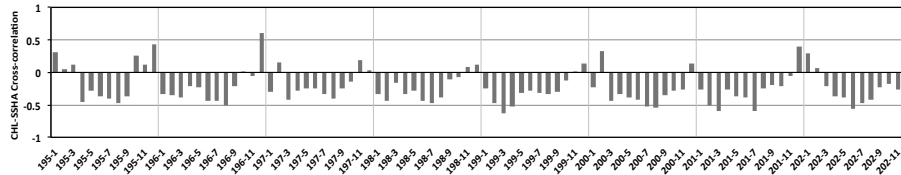
Figure 10. CM2.6 monthly Chlorophyll-SSHA cross-correlation over 8 years within 56–66° E and 15–26° N.

(a) Chlorophyll-a and SSHA at November 9th

(b) Chlorophyll-a and SSHA at December 28th

(c) Chlorophyll-a and SSHA: November and December along 16°N

(d) Chlorophyll-a and SSHA: November and December along 19°N
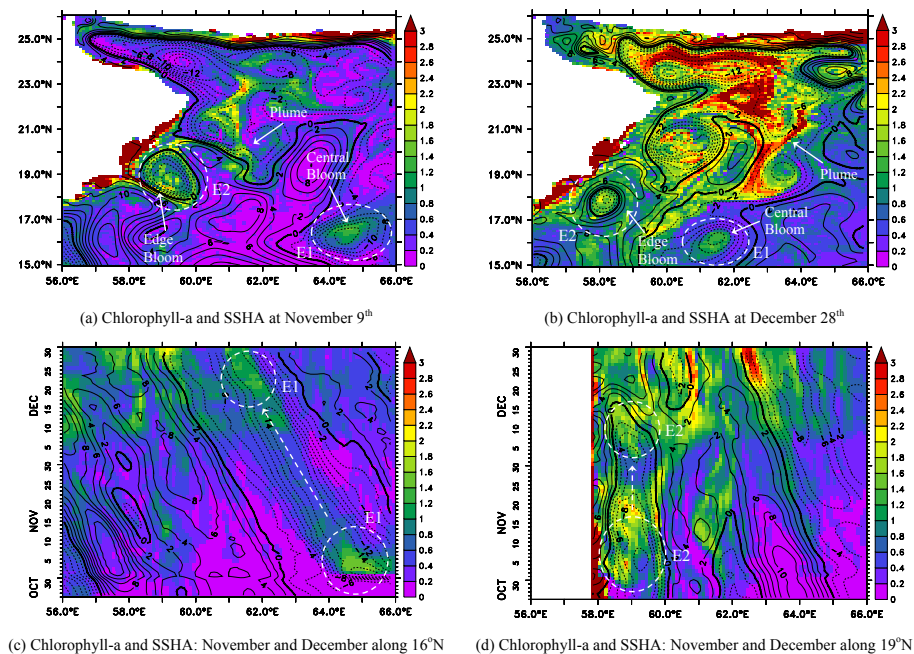
Figure 11. CM2.6 (miniBLING) Surface chlorophyll *a* concentration and sea surface height anomaly (SSHA) November and December during a year where the observed eddy-bloom interaction is seen in the Southern part of the Arabian Sea.
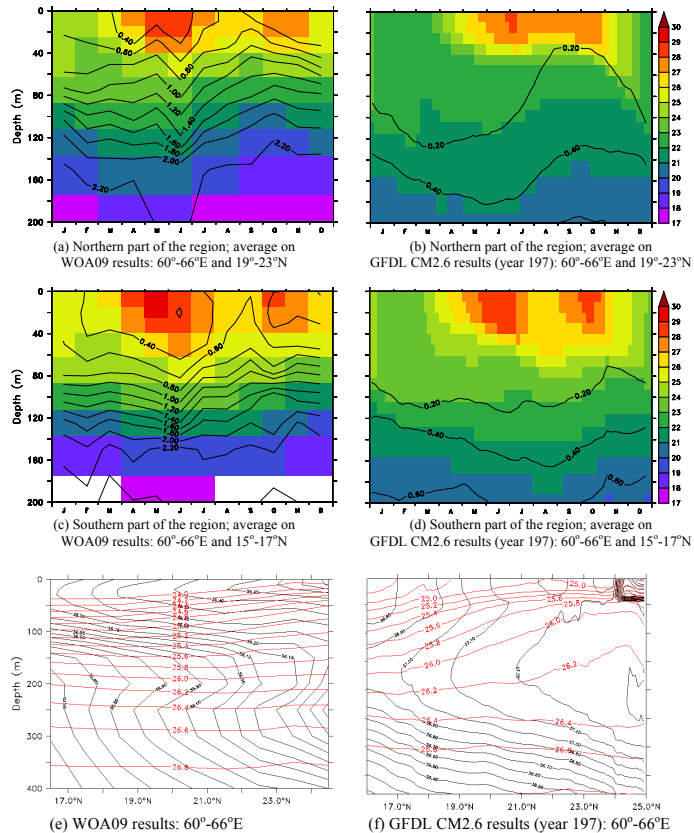
Figure 12. (a)–(d) Seawater temperature (°C) and phosphate (PO$_4$) concentration (contours, µM) for the northern (top row) and southern (middle row) parts of the central Arabian Sea. **(e)**, **(f)** Yearly averaged subsurface distribution of salinity (black contours) and potential density (red contours). Left-hand column shows observations, right-hand column results from CM2.6 model.

Title Page

Abstract | Introduction

Conclusions | References

Tables | Figures
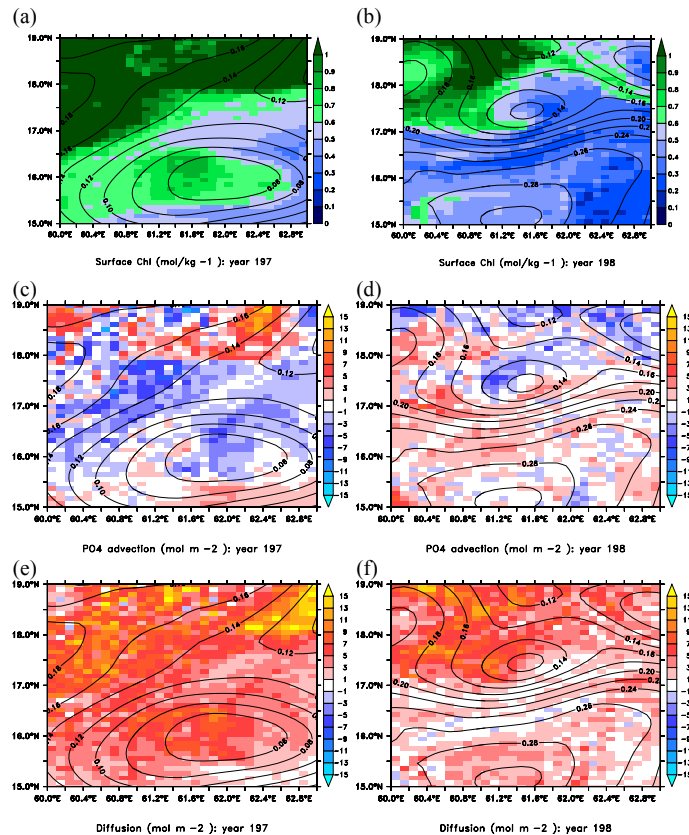
◄ | ►

◄ | ►

Back | Close

Full Screen / Esc

Figure 13. Surface chlorophyll in mg m^{-3}. **(a)**, **(b)** Advective flux of phosphate to top 50 m in mol m^{-2} (**c, d**, colors), and diffusive flux of phosphate in mol m^{-2} (**e, f**, colors) with sea surface height (contours, overlaid) for eddy E1 (63–66° E, 15–18° N) for the month of December during the two CM2.6 model years 197 and 198.

Title Page

Abstract | Introduction

Conclusions | References

Tables | Figures

|◀ | ▶|

◀ | ▶

Back | Close

Full Screen / Esc